International Journal of Biological Macromolecules 56 (2013) 140–148

Contents lists available at SciVerse ScienceDirect

International Journal of Biological Macromolecules

journal homepage: www.elsevier.com/locate/ijbiomac

Structural and stability studies of the human mtHsp70-escort protein 1: An essential mortalin co-chaperone

P.R. Dores-Silva[a], K. Minari[a,b], C.H.I. Ramos[c], L.R.S. Barbosa[d], J.C. Borges[a,*]

[a] Instituto de Química de São Carlos, Universidade de São Paulo – USP, São Carlos, SP 13560-970, Brazil
[b] Centro de Ciências Biológicas e da Saúde, Universidade Federal de São Carlos, São Carlos, SP 13565-905, Brazil
[c] Instituto de Química, Universidade de Campinas – UNICAMP, Campinas, SP 13083-970, Brazil
[d] Grupo de Biofísica, Departamento de Física Geral, Instituto de Física, USP, São Paulo, SP 05508-090 Brazil

ARTICLE INFO

Article history:
Received 20 December 2012
Received in revised form 7 February 2013
Accepted 9 February 2013
Available online 24 February 2013

Keywords:
Hep1
mtHsp70
Mortalin
Fluorescence
Analytical ultracentrifugation
Oligomerization

ABSTRACT

Mitochondrial Hsp70 is involved in both protein import and folding process, among other essential functions. In mammalian cells, due to its role in the malignant process, it receives the name of mortalin. Despite its importance in protein and mitochondrial homeostasis, mortalin tends to self-aggregate *in vitro* and *in vivo*, the later leads to mitochondrial biogenesis failure. Recently, a zinc-finger protein, named Hsp70-escort protein 1 (Hep1, also called Zim17/TIM15/DNLZ), was described as an essential human mitochondrial mortalin co-chaperone which avoids its self-aggregation. Here, we report structural studies of the human Hep1 (hHep1). The results indicate that hHep1 shares some structural similarities with the yeast ortholog despite the low identity and functional differences. We also observed that hHep1 oligomerizes in a concentration-dependent fashion and that the zinc ion, which is essential for hHep1 *in vivo* function, has an important protein-structure stabilizing effect.

1. Introduction

The majority of the mitochondrial proteins are encoded by the nuclear genome, translated by cytosolic ribosomes as preproteins containing peptide signals, leading to its translocation into the mitochondria [1–4]. Therefore, the machineries of import and sorting proteins into mitochondria are consequential in the biogenesis, maintaining suitable mitochondrial functions. For that, mitochondrial molecular chaperones, coordinated by the mitochondrial Hsp70 (mtHsp70), perform a critical role in the mitochondrial import system of matrix proteins. Mitochondrial Hsp70 works as a motor import that drives the preprotein import process and helps the fate and folding of these proteins [4,5]. Similar to cytosolic Hsp70, mtHsp70 presents an N-terminal ATPase domain (NBD) and a C-terminal substrate binding domain (SBD), which are controlled by a reciprocal allosteric mechanism [6].

Mammalian mtHsp70 is also called mortalin due to its activity in senescence and cellular death [7]. Mortalin is involved in several cellular process and may play key roles in Parkinson's and Alzheimer's diseases [7,8], and some cancers [9,10]. Mortalin interacts and kidnaps the wild type p53 in the cytoplasm reducing its transcriptional activity, since mortalin is not an exclusively mitochondrial protein [7,11,12]. Although mortalin has been known for a long time, its structural study is limited due to a self aggregation process when it is produced heterologously [4,13,14]. Aggregation of mtHsp70 leads to defects in protein import into mitochondria and subsequent TIM23 dependent biogenesis failure [13]. Recently, a new mitochondrial Hsp70 co-chaperone was described as Hsp70-escort protein (Hep1 – Zim17/TIM15/DNLZ), given that it has a dual role in mtHsp70: (1) preventing its self-aggregation and (2) controlling its ATPase activity [14,15].

Hep1 is essential for mitochondrial import machinery located in the mitochondria matrix [14,16,17]. The deletion of yeast Hep1 (yHep1) leads to defective import of preproteins dependent on TIM23 complex, which is also required for yeast growth at elevated temperature [14]. However, since Hep1 acts protecting mtHsp70 from aggregation, the defective effects of yHep1 deletion on protein import by mitochondria could be due to mtHsp70 malfunction/aggregation, and not directly linked to Hep1 activity [4,13,14].

Abbreviations: AUC, analytical ultracentrifugation; CD, circular dichroism; DSC, differential scanning calorimetry; f/f_0, frictional ratio; MM, molecular mass; R_s, Stokes radius; R_g, radius of gyration; SAXS, small angle X-ray scattering; $s_{20,w}$, sedimentation coefficient at standard conditions; $s^0_{20,w}$, standard sedimentation coefficient at 0 mg mL^{-1} of protein; [Θ], residual molar ellipticity; ⟨λ⟩, spectral center of mass.

* Corresponding author at: Instituto de Química de São Carlos, Universidade de São Paulo, P.O. Box 780, São Carlos, SP 13560-970, Brazil. Tel.: +55 16 3373 8637; fax: +55 16 3373 9982.
E-mail addresses: borgesjc@iqsc.usp.br, borgesjciqsc@gmail.com (J.C. Borges).

0141-8130 © 2013 Elsevier B.V. Open access under the Elsevier OA license.
http://dx.doi.org/10.1016/j.ijbiomac.2013.02.009

In yeast, Hep1 binds specifically to the NBD of mtHsp70 preventing its self-aggregation in a substoichiometric way [14,18,19], but it may need the interdomain linker of mtHsp70 to properly bind [20].

Hep1 contains a zinc-finger domain which is critical for its *in vivo* function, in both yeast and human cells [17,21]. The nuclear magnetic resonance (NMR) structure of yHep1 shows an L-shape where the zinc-finger cluster is quite buried and forms the major leg, and two small α-helices form the other leg of unknown function [22]. Deletion or modifications of the zinc finger motif of human Hep1 (hHep1) leads to defects in the aggregation avoidance action of mortalin, suggesting that the zinc-finger cluster of hHep1 is also essential for its interaction with mortalin [21].

Although hHep1 can supplement *in vivo* yHep1 deletion [21], these proteins are not functionally equivalent. It was shown that hHep1 increases human mortalin ATPase activity [15,18,19,21], however this activity was not observed in yHep1 [14]. It was also reported that hHep1 interacts with the helical lid of mortalin and also with the NBD, which stimulates the ATPase activity of mortalin in a mutually exclusive manner with Hsp40 proteins [15]. Interestingly, yHep1 prevents human mortalin aggregation, suggesting that the mechanism of action of Hep1 is conserved in these proteins [18]. Besides, there are evidences that hHep1 presents intrinsic chaperone activity [15].

In this study, we characterized the structure and stability of hHep1 using biophysical tolls. First of all, recombinant hHep1 prevented recombinant human mortalin aggregation in a coexpression system. Human Hep1 was purified folded and behaved mainly as an asymmetric monomer, but it also oligomerized in a concentration dependent manner. Disturbing the hHep1 structure in the presence and absence of the EDTA, we demonstrate that the zinc ion of the zinc-finger domain, which is essential for hHep1 *in vivo* function [17], plays a stabilizing role in the hHep1 structure.

2. Material and methods

2.1. Cloning, expression and purification

The EST clone (dbEST Id: 14322301) was obtained from the IMAGE consortium and was used as template for amplification of hHep1 DNA coding (Genbank accession number NP_001074318.1). We used a specific forward primer (5′-ATTCATATGAGCTCCGAGCAGGGGCCG-3′) to amplify hHep1 DNA and to create a restriction site for *Nde* I downstream of the mitochondrial peptide signal (sequence Met1-Ser49 predicted by the MITOPROT program [23]). This strategy eliminated the peptide signal of the recombinant protein. The T7 primer, which anneals in the pOTB7 vector, was used as reverse primer. Using the *Nde* I and *Kpn* I restriction enzymes, the hHep1 DNA was inserted into pQE2 expression vector (Qiagen), resulting in the vector pQE2::hHep1 which codifies hHep1 containing a His-tag sequence (MKHHHHHHH) at the N-terminal of the protein.

Human mortalin was cloned from the EST clone (dbEST Id: 6195001) using the forward (5′TATGCATCACATATGATCAAGGGAGC3′) and reverse primer (5′ATTTCTGGGATCCTTACTGTTTTCC3′) containing restriction sites for *Nde* I and *Bam*H I, respectively. The forward primer of the mortalin was designed to eliminate the mitochondrial peptide signal (sequence Met1-Ala47 also predicted by the MITOPROT program [23]). The DNA insert was cloned into pET28a expression vector generating the vector pET28a::Mortalin also able to express mortalin fused to a His-tag sequence. The cloning processes were confirmed by DNA sequencing.

The recombinant proteins were expressed in *Escherichia coli* BL21(DE3) strain. Summarily, cells transformed with pQE2::hHep1 were grown at 37 °C in LB medium, containing ampicillin 35 μg mL^{-1}, to an OD_{600nm} (optical diffraction at 600 nm) of 0.5 where the protein expression was induced by 0.2 mM of isopropyl thio-β-D-galactoside (IPTG) at 30 °C. After 4 h of induction, the cells were harvested by centrifugation at 2600 × *g* for 10 min. Mortalin was expressed in *E. coli* BL21(DE3) strain in LB medium containing kanamycin 35 μg mL^{-1}, to an OD_{600nm} of 0.5 where the protein expression was induced by 0.2 mM of IPTG. After 18 h of induction at 23 °C, the cells were harvested by centrifugation at 2600 g for 10 min. Mortalin and hHep1 coexpression assays were performed in *E. coli* BL21(DE3) strain in LB medium containing both ampicillin and kanamycin at 35 μg mL^{-1}. The cells were grown at 37 °C until an OD_{600nm} of 0.5, at which time the temperature was reduced to 23 °C, and IPTG was added to a final concentration of 0.2 mM. The cells were incubated for 18 h at 200 rpm, harvested by centrifugation at 2600 × *g* and stored at −20 °C.

For cell lyses, the induced pellet was suspended in 50 mM Tris–HCl (pH 8.0), 100 mM KCl and incubated with 30 μg mL^{-1} of lysozyme (Sigma) and 5 U of DNAse (Promega) on ice for 30 min. The pellet was disrupted by sonication and centrifuged at 20,000 × *g* for 30 min at 4 °C. The supernatant was submitted to a nickel affinity chromatography in a HisTrap column (GE Healthcare Life Sciences) and further purification was performed in a Superdex 200 pg column (GE Healthcare Life Sciences), both coupled to an ÄKTA Prime system (GE Healthcare Life Sciences) in TKP buffer (25 mM Tris–HCl, pH 7.5, 50 mM NaCl, 5 mM sodium phosphate, 5 mM KCl and 2 mM β-mercaptoethanol). The expression and purification processes efficacy were checked by SDS-PAGE. The protein concentration was determined spectrophotometrically, using the calculated extinction coefficient for native conditions.

2.2. Homology molecular modeling

The hHep1 (Gly62-Ala160) structure was modeled with homology-modeling using the Swiss Model server [24]. The solution structure of the truncated yHep1 solved by NMR (PDB accession no 2E2Z) was used as template.

2.3. Spectroscopy studies

Circular dichroism (CD) measurements were performed in a Jasco J-810 spectropolarimeter. Human Hep1 was tested in TKP, at final concentrations ranging between 20 and 70 μM in the absence and presence of 2 mM EDTA, using a circular 0.2 mm pathlength cuvette. The spectra were normalized to residual molar ellipticity ([Θ]) and the protein secondary structure content was estimated by the CDNN Deconvolution program [25].

Intrinsic fluorescence emission measurements were performed in an F-4500 fluorescence spectrophotometer (Hitachi), using a 10 mm × 2 mm pathlength cell with hHep1 in TKP buffer, at 20 °C. The fluorescence emission spectra were measured from 300 to 420 nm, after excitation at 280 nm, at hHep1 concentrations (as a monomer) ranging between 5 and 350 μM (74–5200 μg mL^{-1}). Experiments in the absence and presence of increasing concentrations of urea or guanidine-hydrochloride (Gnd-HCl) were performed with hHep1 concentration of 15 μM. The urea and Gnd-HCl solutions were prepared in TKP buffer. The chemical-induced unfolding was also performed in the presence of 2 mM EDTA after 60–120 min equilibrium time, at 20 °C. The data were analyzed by maximum fluorescence emission wavelength (λ_{max}) and spectral center of mass ($\langle\lambda\rangle$), as described by the equation below:

$$\langle\lambda\rangle = \frac{\sum \lambda_i F_i}{\sum F_i} \quad (1)$$

where λ_i represents each wavelength observed and F_i represents the fluorescence intensity at each wavelength. The urea induced

unfolding curves were fitted with a Double-Boltzmann Function, available in the Origin program (Microcal), in order to obtain the concentration at the midpoint of the urea-induced unfolding transition – C_m,

2.4. Hydrodynamic characterization

The Superdex 200 GL 10/30 column (GE Healthcare Life Sciences), coupled to an ÄKTA Prime system, was used to carry out analytical size exclusion chromatography (aSEC) experiments. hHep1 samples at several protein concentrations were applied onto the column previously washed with TKP buffer. The column was calibrated with standard protein mixture (at ~1 mg mL^{-1}) of known Stokes radii (R_s): apoferritin (67 Å); γ-globulin (48 Å), bovine serum albumin (36 Å), ovalbumin (30 Å), carbonic anhydrase (24 Å) and cytochrome c (14 Å). The retention times were transformed in the partial coefficient k_{av} applying the following equation:

$$k_{av} = \frac{V_e - V_0}{V_t - V_0} \quad (2)$$

where V_e is the elution volume of the protein; V_0 is the void volume of the column and the V_t is the total volume of the column. The $-\log k_{av}$ was plotted against the R_s in order to estimate the R_s of hHep1 by linear regression.

Analytical ultracentrifugation (AUC) experiments were performed in a Beckman Optima XL-A analytical ultracentrifuge. Sedimentation velocity experiments for hHep1 were carried out in concentrations of 150–2500 μg mL^{-1} in TKP buffer, at 20 °C, 35,000 rpm (AN-60Ti rotor), and data acquisition at 236 nm (low concentrations) and 277 nm (high concentrations). The absorbance *versus* cell radius data were fitted by the software SedFit (Version 12.1) [26]. As a regularization parameter, the frictional ratio (f/f_0) was allowed to float freely. The sedimentation coefficients were obtained as the maximum of the peaks of the c(S) curves and converted to standard conditions ($s_{20,w}$) [27]. The TKP buffer viscosity ($\eta = 1.0145 \times 10^{-2}$ poise), density ($\rho = 1.00183$ g mL^{-1}) and partial-specific volume ($V_{bar} = 0.7230$ mL g^{-1}) were estimated by the Sednterp program (http://www.jphilo.mailway.com/download.htm). With the $s_{20,w}$-value at each protein concentration the standard sedimentation coefficient was estimated at 0 mg mL^{-1} of protein concentration ($s^0_{20,w}$) by linear regression [27]. The f/f_0 can also be estimated by the ratio of the experimental R_s to the radius of a sphere of the same mass, or by the ratio of the sedimentation coefficient of a sphere of the same mass to the experimental one [27].

2.5. Small angle X-ray scattering experiments

Small angle X-ray scattering (SAXS) experiments were performed in the Laboratório Nacional de Luz Síncrotron (LNLS, Campinas-SP, Brazil) using a monochromatic X-ray beam (wavelength of λ = 1.488 Å) of the D02A-SAXS2 beamline. The sample-to-detector distance was of ~1000 mm, which corresponds to the scattering vector range of $0.015 < q < 0.35$ Å^{-1}, where q is the magnitude of the q-vector defined by $q = (4\pi/\lambda)\sin\theta$ (with 2θ as the scattering angle). Human Hep1 samples were placed in a 1-mm path length cell formed by two mica windows, and the scattering curves were recorded at different sample concentrations (1.7–8.6 mg mL^{-1}) solved in TKP buffer. Samples and buffers were submitted to X-ray frames of 300 s. The scattering curves were corrected for detector response and scaled by the incident beam and attenuated intensity of the sample. The corrected sample scattering was subtracted from the buffer scattering curve. All intensities are in absolute scale, cm^{-1}, such calibration was established from the scattered intensity of pure water, which depends on the isothermal compressibility and on its electron density ($I(0)_{water}$, $_{293\,K} = 0.01632$ cm^{-1}) [28]. The $I(0)$ value is related to the protein concentration as well as to MM and consequently to the protein aggregation state. Thus the $I(0)/c_{prot}$ (where c_{prot} is the protein concentration) and the protein radius of gyration, R_g, can give useful information on the protein aggregation state [29]. The urea effect on the hHep1 (at 3.5 mg mL^{-1}) structure was also checked by SAXS in the absence and presence of 2 mM EDTA, measuring samples composed of 0 and 6 M of urea. All scattering curves were carefully corrected by the urea-containing buffer.

2.6. Differential scanning calorimetry

Differential scanning calorimetry (DSC) measurements of thermal-induced unfolding were performed in a Nano DSC (TA Instruments). The measurements were performed at 1.5 mg mL^{-1} solved in TKP buffer after extensive dialysis. The scan rate tested was of 1.0 °C min^{-1} at the 20–90 °C temperature range. The reversibility of thermal unfolding was tested by performing several consecutive up/down scans. The experimental thermograms were collected with DSCrun software (TA Instruments) and analyzed using the NanoAnalyze software (TA Instruments). The baselines were calculated from the pre- and post-transition temperature regions.

3. Results and discussion

3.1. Recombinant human mortalin aggregation is prevented by hHep1 coexpression

The hHep1 DNA coding (gi|124249391) was cloned into the pQE2 expression vector without the corresponding mitochondrial peptide signal sequence. Therefore, hHep1 construction consists of the Ser50-Ser178 amino acid sequence (Fig. S1–supplementary material). The recombinant hHep1 was expressed in high levels and partially soluble after cell lysis (Fig. 1A). The recombinant protein was purified by 2 chromatographic steps (see Section 2 for details), thereby obtaining high purity hHep1 (lane 7 – Fig. 1A).

The functionality of the recombinant hHep1 was analyzed for its ability to maintain recombinant human mortalin solubility in a coexpression system. Fig. 1B shows the expression of recombinant human mortalin in the absence of hHep1, which yielded the protein in the insoluble fraction of lysed cells and a minor part in the supernatant (Fig. 1B – comparison on lanes 3, 4 and 5, respectively). When mortalin and hHep1 were coexpressed, mortalin was found in much of the supernatant of the lysed cells (Fig. 1B – comparison of lanes 7, 8 and 9, respectively). This functional result suggests that hHep1 solubilized the recombinant human mortalin, as was previously shown [14,18,19,21], allowing the production and purification of mortalin in the monomeric state (data not shown).

3.2. Recombinant hHep1 was produced folded

The secondary structure content of hHep1 was studied by CD spectropolarimetry (Fig. 1C). As observed for the zinc-finger domain truncations of hHep1 [21], hHep1 presented CD spectra with a minima signal at 207 nm and a shoulder at 220 nm. The secondary structure estimation performed by the CDNN Deconvolution software [25] suggested that hHep1 is formed by 10% of α-helices, 34% of β-sheet and 21% and 35% of turns and random coils, respectively. The solution structure of the truncated yHep1, solved by NMR, suggests that the secondary content is of about 23% and 28% of α-helices and β-sheets, respectively, with similar CD spectra [22]. Based on these data, we can conclude that hHep1 is mainly formed by β-sheets, which involves the zinc-finger domain

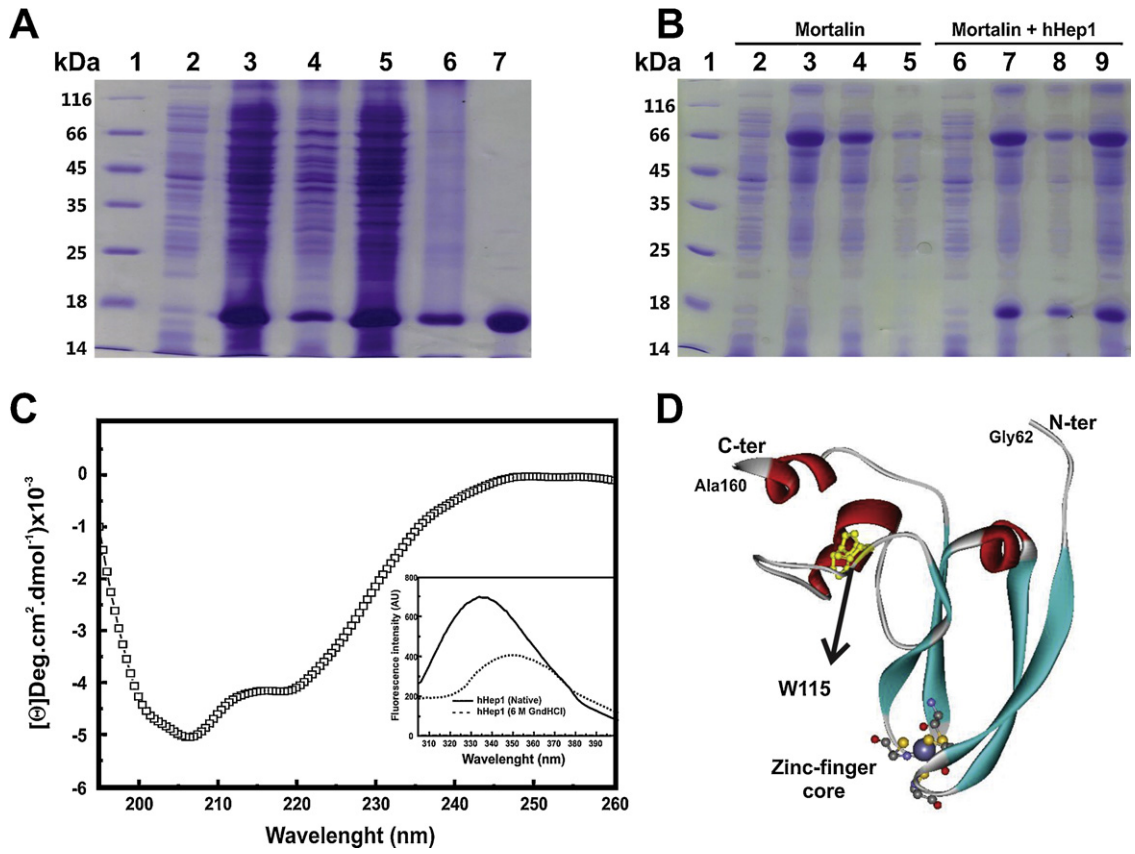

Fig. 1. hHep1 production, purification, functional and spectroscopic assays. (A) The picture depicts a SDS-PAGE 13.5% showing that hHep1 remains in the soluble fraction after cell lysis and that it was purified until homogeneity. (1) MM markers (left); (2) non-induced bacterial pellet; (3) induction bacterial pellet; (4) cell lysate pellet; (5) cell lysate supernatant, (6) eluate from the nickel affinity chromatography; and (7) hHep1 after size exclusion chromatography. (B) hHep1 was able to maintain recombinant human mortalin in the soluble fraction of the lysed cells. Mortalin was expressed alone (lanes 2–5) and coexpressed with hHep1 (lanes 6–9) as described in Section 2. (1) MM markers (left); (2) non-induced bacterial pellet; (3) induction bacterial pellet; (4) cell lysate pellet; and (5) cell lysate supernatant; (6) non-induced bacterial pellet of the coexpression; (7) induced bacterial pellet of the coexpression; (8) cell lysate pellet of the coexpression; (9) cell lysate supernatant of the coexpression. (C) hHep1 secondary and tertiary structures were analyzed by circular dichroism and intrinsic emission fluorescence, respectively. Mean residue ellipticity [Θ] spectra suggested that hHep1 is mainly formed by β-sheet structure (see text for details). *Inset*: hHep1 intrinsic fluorescence emission experiments were performed with 15 μM of protein solved in the TKP buffer and excitation wavelength at 280 nm. The spectra showed that the single Trp residue of hHep1 was partially exposed to the solvent and exhibited λ_{max} and $\langle\lambda\rangle$ of 336(1) nm and 344.7(0.1) nm, respectively. In the presence of 6 M GndHCl, hHep1 showed λ_{max} and $\langle\lambda\rangle$ of 350(1) nm and 354.2(0.3) nm, respectively. Altogether, these results attested the production of hHep1 in both folded and functional state. (D) hHep1 (62–160) was modeled using the Swiss-model program and the truncated yHep1 structure (PDB accession no 2E2Z) as template. The structure shows the position of the Trp115 (yellow) of the hHep1 and the zinc-finger domain where the Cys residues which form the zinc-finger motif are presented. The zinc ion is shown in blue.

as observed for yHep1. This data indicates that hHep1 and yHep1 share similarities in the secondary structure level, in spite of their identity (25%) in the amino acid sequence (Fig. S1 – supplementary material and [19]).

Intrinsic fluorescence emission spectrophotometry was used to obtain information on the local tertiary structure of hHep1, since it has a single Trp115 residue, which was used as a fluorescent probe (Fig. S1 – supplementary material). Fig. 1C (*inset*) shows the hHep1 (15 μM) fluorescence emission spectra in native and in denaturant conditions (6 M Gnd-HCl). The results showed that hHep1, in native conditions, presents a λ_{max} centered at 336(1) nm and a $\langle\lambda\rangle$ of 344.7(0.1) nm. In the presence of 6 M Gnd-HCl, hHep1 presented λ_{max} and $\langle\lambda\rangle$ centered at 350(1) and 354.2(0.3) nm, respectively, suggesting that it unfolded by 6 M Gnd-HCl. These results indicated that hHep1 can exhibit the Trp115 residue partially exposed to the solvent. The hHep1 homology model (Fig. 1D), in spite of the low confidence due to the low identity of hHep1 and the template yHep1, indicates that Trp115 is partially buried between two α-helices in the hHep1 C-terminal region, supporting the experimental data. Overall, the purification and spectroscopy data suggest hHep1 was purified until homogeneity and at its folded state.

3.3. Human Hep1 oligomerizes in a concentration-dependent mode

We studied the hydrodynamic properties of hHep1 using aSEC technique (Fig. 2A). At 2 mg mL^{-1} (~135 μM), hHep1 showed an elution profile compatible with a MM of carbonic anhydrase, suggesting that it could be a globular dimer. The experimental R_s determined for hHep1 was of 22(1) Å (Fig. 2A, *inset*) and the theoretical R_s for a globular protein of 14.8 kDa (MM of hHep1 as a monomer) and 29.6 kDa (MM of hHep1as a dimer) are of about 16 Å and 20 Å, respectively (Table 1). Taken together, the aSEC data observed for hHep1 suggest that it can be a globular dimer or an asymmetric monomer. Similar results were observed for the truncated forms of hHep1 [21].

In order to get further information on the hydrodynamic and structural parameters of hHep1 in solution, we performed sedimentation velocity AUC experiments with hHep1 in the concentration range of 0.15–2.5 mg mL^{-1} (~10–170 μM). Fig. 2B shows the continuous c(S) distribution suggesting that hHep1 exhibits one predominant species and, at least, 3 other species in solution (Fig. 2B, *inset*). The predominant particle observed for hHep1 sedimentation velocity data provided a $s^0_{20,w}$ of 1.62(2) S (Fig. 2C)

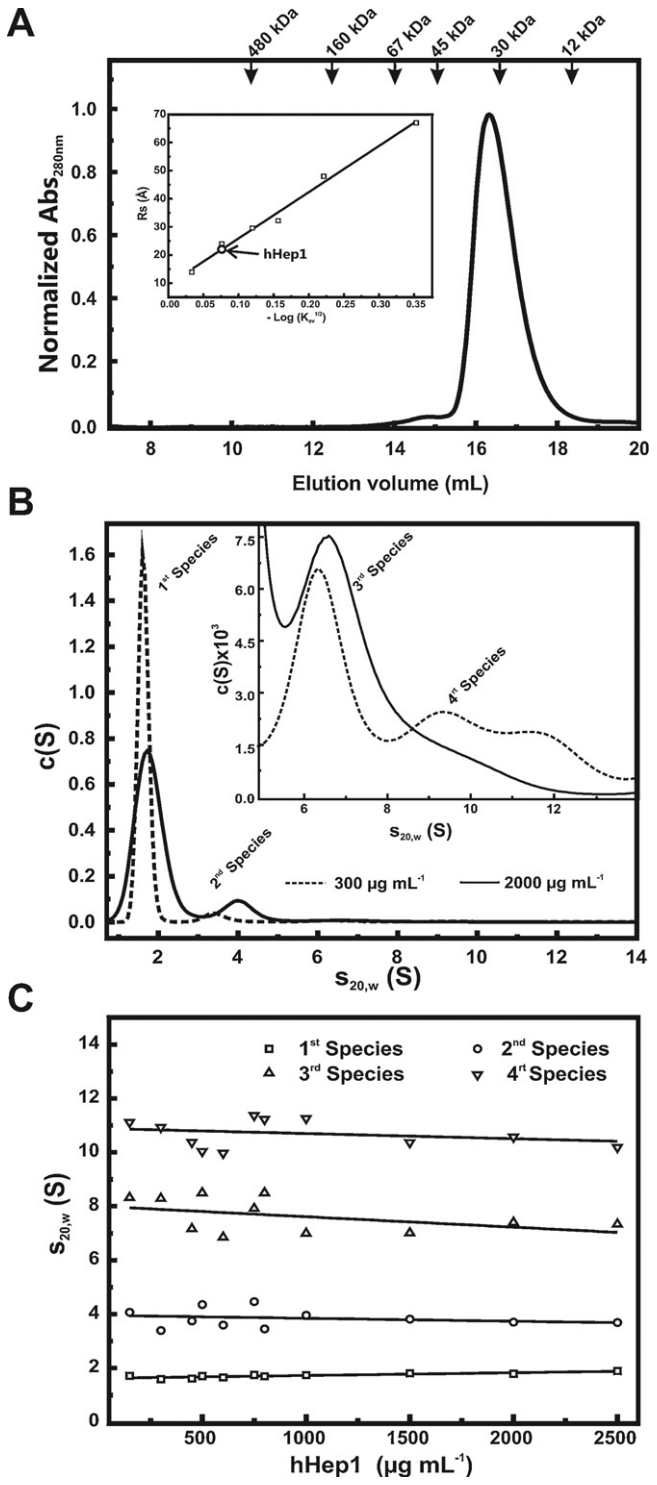

Fig. 2. hHep1 behaves as a mixture of monomers and oligomers species. (A) Analytical SEC experiments showed that hHep1 eluate with an apparent MM of about 30 kDa as anhydrase carbonic did. *Inset*: the retention volume observed for the standard proteins were transformed in the partial coefficient k_{av} (Eq. (2)) and plotted against the R_s of the standard proteins. The arrow shows the partition coefficient of hHep1 and corresponds to 22(1) Å. (B) The figure depicts the continuous c(S) distributions in 2 protein concentrations where maximum of peaks resulted in $s_{20,w}$. At least 4 species could be observed in the c(S) distributions. *Inset*: zoom in the $s_{20,w}$ range 5–13 S showing the presence of peaks with higher $s_{20,w}$-values. (C) Figure depicts the plot of $s_{20,w}$ *versus* protein concentration of the four main species observed in the sedimentation velocity data. All curves were fitted by linear regression in order to calculate $s^0_{20,w}$ for all four species observed (Table 1). The sedimentation velocity data suggest that hHep1 is the equilibrium of many oligomers and that it undergoes oligomerization in a concentration-dependent manner (see text for details).

Table 1
Hydrodynamic properties of hHep1.

hHep1	hHep1 hydrodynamic properties		
	MM (kDa)	*Rs* (Å)	$s^0_{20,w}$ (S)
Predicted			
Monomeric sphere	14.8	16	2.24
Dimeric sphere	29.6	20	3.55
aSEC	30(2)	22(1)	–
Sedimentation velocity AUC experiments			
1st species	15(1)	–	1.62(0.02)
2nd species	57(6)	–	3.9(0.2)
3rd species	170(20)	–	8.0(0.3)
4th species	290(20)	–	10.9(0.3)

and the MM calculated by the SedFit software was of about 15 kDa (Table 1), suggesting that it is the monomeric form of hHep1. Based on the $s^0_{20,w}$ and MM values estimated for other species present in the hHep1 solution, the second species can be a tetramer with a $s^0_{20,w}$ of 3.9(0.2) S and 57 kDa. The third species has a $s^0_{20,w}$ of 8.0(0.3) S and can be a decamer-dodecamer, while the forth species ($s^0_{20,w}$ of 10.9(0.3) S) is a larger oligomer that can contain around 16–20 units of hHep1. Since there is a low quantity of these two last species in solution, our data is unable to accurately define the stoichiometry. It is worth mentioning that the f/f_0, obtained by the ratio of the *s*-value calculated for a spherical particle of 14.8 kDa by the experimental $s^0_{20,w}$-value of the smallest particle, was of around 1.4, hence suggesting that the monomeric form of hHep1 in solution is slightly elongated. This observation is in agreement with the solution structure solved for the truncated yHep1, which also shows an asymmetric shape [22], and the modeled hHep1 structure (Fig. 1D).

The sedimentation velocity data indicated that hHep1 as monomer should be the main particle in solution. We detected that, at 150 µg mL^{-1} (~10 µM), hHep1 monomer is about 92–93% of relative mass in solution, as observed in the relative area under the c(S) curve ratio. Furthermore, it decreases to around 75% at 2.5 mg mL^{-1} (~170 µM). On the other hand, the relative amount of the oligomers increases as a function of hHep1 concentration (Fig. 3A). For instance, the amount of hHep1 as tetramer increased from 5% at 150 µg mL^{-1} to 16% at 2.5 mg mL^{-1}, while the amount of decamer-dodecamer increased from 2% up to 6% at the same protein concentration range. The larger oligomer was less than 1% of the protein mass in the protein concentration range tested (data not shown). These results indicated that the second and third species concentrations increased 3-fold at the concentration range tested. Interestingly, high NaCl concentrations (250–750 mM) led to a slight dissociation effect of the hHep1 oligomers. However, it did not change the hHep1 c(S) distribution profile since all 3 aforementioned oligomer forms remained present in solution, as observed by AUC experiments (data not shown). Overall, the hydrodynamic characterization experiments suggest that hHep1 oligomerizes in a protein concentration mode.

We also studied hHep1 by means of SAXS technique, through the forward scattering intensity value, $I(0)$, which can provide the MM, if the sample is monodisperse [30]. However, it is not the case of hHep1 based on the sedimentation velocity data. Thus, the SAXS data are analyzed using the $I(0)/c_{prot}$ value, which can yield interesting information on the protein aggregation state [31]. A consistent increment of the $I(0)/c_{prot}$ value was observed with the increasing protein concentration (Fig. 3B), indicating that hHep1 oligomerizes as a function of protein concentration. Furthermore, one should bear in mind that the $I(0)/c_{prot}$ value can also indicate the presence of interference effects over the SAXS curve. For instance, one can infer that repulsive interference effects take place over the SAXS curve if such value decreases as the protein concentration increases [32], which is not the case (data not shown). The

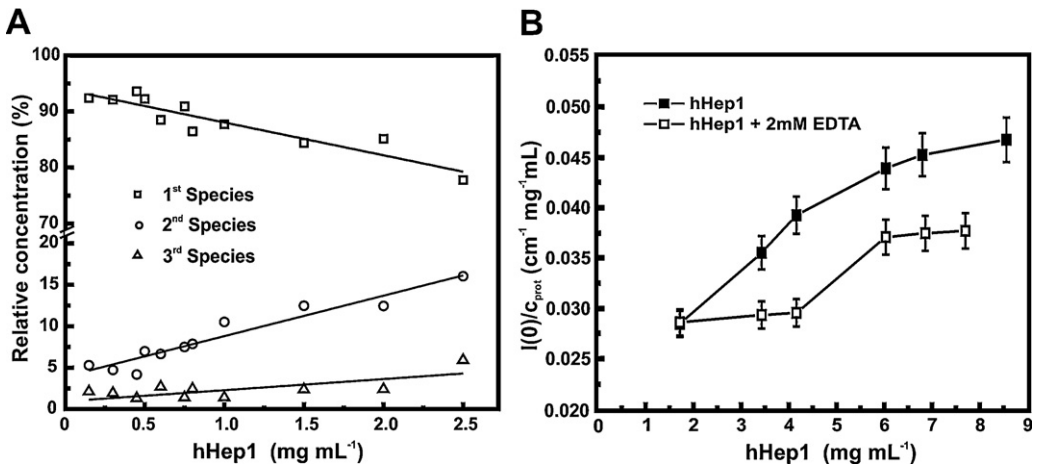

Fig. 3. hHep1 oligomerizes in dependence of the concentration. (A) The relative amount of the three main hHep1 species in solution observed in the AUC experiments, determined by the c(S) distribution data, as a function of the protein concentration. The relative amount of each species was estimated by the ratio of the area under curve of the peak of interest in the c(S) distribution curve by the sum of the area under curve of all peaks in the c(S) distribution curve. The data are presented in percentages. (B) SAXS experiments of hHep1 as a function of protein concentration. hHep1 sample was prepared in TKP buffer (in the absence and presence of 2 mM EDTA) and measured by SAXS in different concentrations of protein (from 1.7 to 8.6 mg mL^{-1}). The I(0) was determined from the Guinier region of the scattering curve (using the plot LnI(0) *versus* q^2), in this case the I(0) is the linear coefficient.

$I(0)/c_{prot}$ value increases from 0.028 up to 0.046 cm^{-1} mg^{-1} mL for 1.5 and 8.5 mg mL^{-1}, respectively (Fig. 3B), it is almost a two-fold increase in the $I(0)/c_{prot}$ value. The R_g, however, increases from 37 Å to 40 Å for 1.5 and 8.5 mg mL^{-1}, respectively (data not shown), indicating that the monomeric species is probably predominant at this concentration range.

Interestingly, in the presence of 2 mM EDTA, hHep1 also exhibited the aforementioned oligomerization dependent on protein concentration; however this effect was less extensive and suggested that some of the hHep1 oligomeric species may be destabilized by the presence of EDTA (Fig. 3B). In this case, the $I(0)/c_{prot}$ value is kept unaltered up to ~4 mg mL^{-1}, after which there this value also increases, indicating that an oligomerization process takes place over the SAXS curves (Fig. 3B).

We also measured the intrinsic fluorescence emission spectra and calculated the ⟨λ⟩-signal as a function of hHep1 concentration (Fig. 4). The normalized hHep1 fluorescence showed a consistent blue shift when the protein concentration increased from 5 μM (74 μg mL^{-1}) to 50 μM (740 μg mL^{-1}), and to 350 μM (5.2 mg mL^{-1}) (Fig. 4A). The ⟨λ⟩-signal as a function of hHep1 concentration also showed a consistent blue shift, in which the ⟨λ⟩-value decreased around 3 nm at the concentration range tested and stabilized at around 300 μM of hHep1 (Fig. 4B). Moreover, these results promptly suggest that hHep1 oligomerization surface should involve, to some extent, the participation of the Trp115 residue that becomes more protected from the solvent, as well as the oligomerization of hHep1.

3.4. Zinc-finger domain of hHep1 has a structural stabilizing role

In order to understand the hHep1 structural organization we performed urea-induced unfolding experiments followed by intrinsic fluorescence emission (through ⟨λ⟩-signal). It should be noted that the single Trp115 of the hHep1 construction is eleven amino acids after the second hHep1 zinc-finger motif, which could report events that involve the zinc-finger core (Fig. 1D). Human Hep1 chemical-induced unfolding monitored by fluorescence was only partially reversible (data not shown).

As here there was also the concern to evaluate the role of the zinc ion on hHep1 structure, we performed chemical-induced unfolding experiments in the absence and presence of 2 mM EDTA. It was previously, we observed that titration of EDTA (1–100 mM)

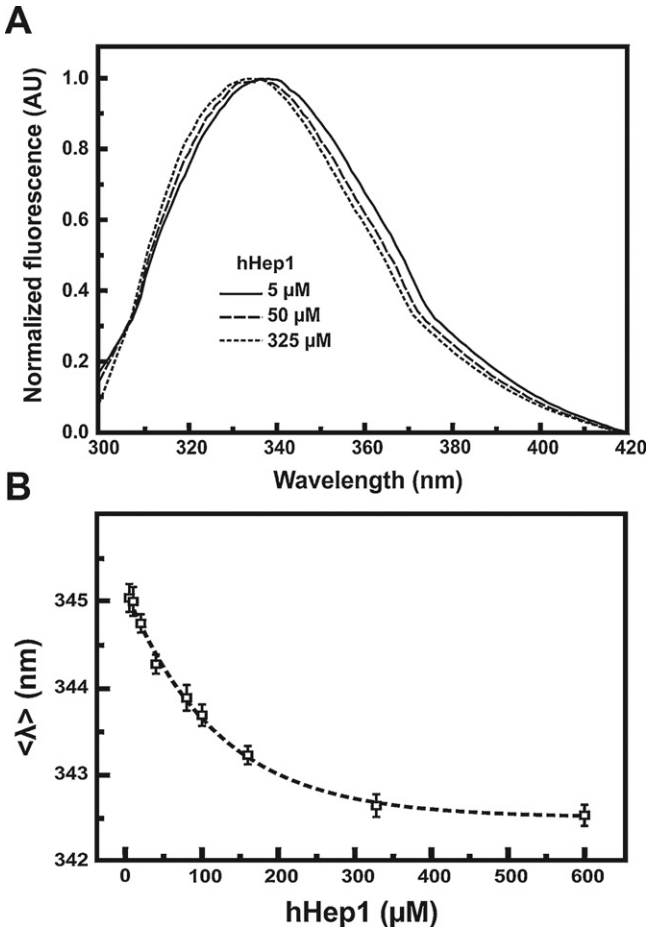

Fig. 4. hHep1 oligomerization surface involves the Trp115. (A) Intrinsic emission fluorescence experiments at different hHep1 concentrations were performed with hHep1 prepared in TKP buffer and excitation wavelength at 280 nm. The normalized intrinsic emission fluorescence spectra show that hHep1 spectra exhibited a blue shift in the high protein concentration samples. (B) The calculated ⟨λ⟩ signals as a function of hHep1 concentration present a consistent blue shift. These results suggest that hHep1 oligomerization involves the Trp115 region surface.

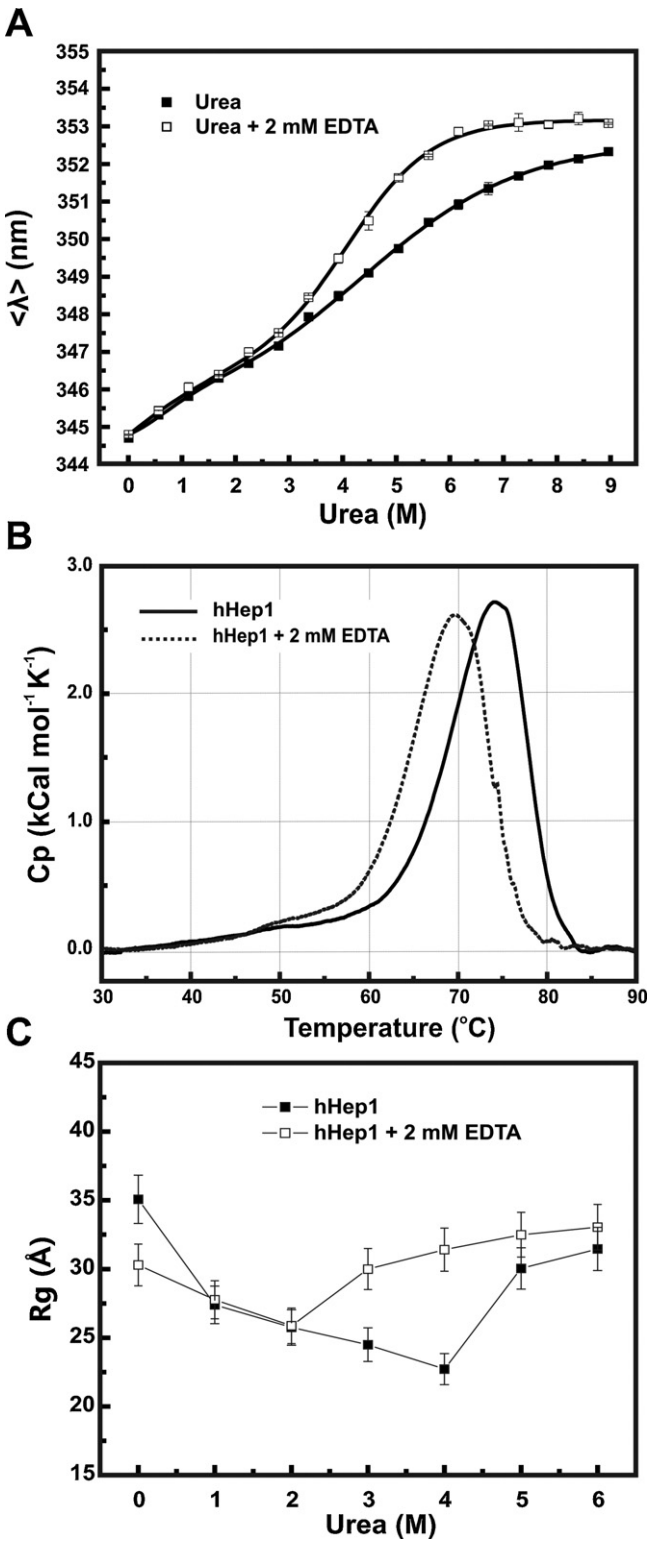

Fig. 5. Zinc ions play a stabilizing role in the hHep1 structure. (A) hHep1 urea-induced unfolding experiments were performed using 15 μM of protein in the absence and presence of 2 mM EDTA (see Section 2 for more details) followed by ⟨λ⟩-signal. In the absence of EDTA, hHep1 urea-induce unfolding was non-cooperative or gradual, suggesting the presence of unfolding intermediates. In the presence of 2 mM EDTA, we observed a shift of the curve to lower urea concentrations, suggesting that EDTA disturbed the stability of the zinc-finger core of hHep1 by chelating the zinc ions. (B) Thermal-induced unfolding followed by DSC experiments of hHep1 in the absence and presence of 2 mM EDTA. Human Hep1 presented a main unfolding transition centered at 74 °C and a shoulder at 50 °C. In the presence of 2 mM EDTA, the main unfolding transition was reduced to 69 °C suggesting that the Zn^{2+} chelating by EDTA destabilized the hHep1 structure. No significant changes were observed in the shoulder centered at 50 °C which should be related to the unfolding intermediates. (C) Weighted-average R_g determined by Guinier's law (*inset*) of hHep1 (at 3.5 mg mL^{-1}) as a function of urea concentration (0 to 6 M) in the absence and presence of 2 mM EDTA. The range of q^2 used to calculate the weighted-average R_g was of 0.00026–0.00084 Å^{-1}, consistent with the validity of Guinier's law, i.e., for $q_{max}.R_g < 1.3$. The curves show a dual effect where first the weighted-average R_g reduces due to the dissociation of the oligomers, and after it increases due to hHep1 unfolding. In the presence of 2 mM EDTA, hHep1 reached its unfolded state earlier than in its absence.

in the hHep1 solutions did not induce changes in the ⟨λ⟩-signal (Fig. S2 – supplementary material). Fig. 5A depicts ⟨λ⟩-signal of hHep1 (at 15 μM) as a function of urea concentration, which show that urea-induced unfolding experiments did not lead hHep1 to the full unfolding. When the same experiment was carried out with Gnd-HCl as chemical denaturant, the ⟨λ⟩-signal reached values higher than 9 M urea (Fig. S3 – supplementary material). This result suggests that hHep1 has high structural stability on urea-induced unfolding.

Fig. 5A also shows that hHep1 urea-induced unfolding had an uncooperative or gradual unfolding profile with no clear transition. When we performed this experiment in the presence of 2 mM EDTA, the gradual transition remained at low urea concentrations, but a more defined transition centered at 3.9 (0.1) M urea was observed. This result suggests that EDTA affected the structure of hHep1, probably by chelating zinc ions and removing them from hHep1 structure, as well as the unfolding of the protein. Thus, urea and 2 mM EDTA had synergistic effects on inducing hHep1 to unfold. Furthermore, the transition centered at 3.9 M urea is the zinc finger core unfolding. The gradual profile observed at low urea concentrations involves the unfolding of some protein region leading to the formation of an unfolding intermediate, consisted by the zinc finger core of hHep1. On the other hand, the hHep1 region, which unfolds at low urea concentration, probably involves the participation of the Trp115 residue. The hHep1 homology model (Fig. 1D) shows that the Trp115 is located between 2 α-helices, suggesting that they could be the hHep1 structural elements that unfold at low urea concentration.

The chemical-induced unfolding experiments using Gnd-HCl as denaturant evidenced the same effect observed for urea in the presence and absence of EDTA, where in the presence of EDTA the unfolding curve changed to lower denaturant concentration (Fig. S3 – supplementary material). Therefore, zinc ion has a structural impact on the stabilization of hHep1.

Differential scanning calorimetry experiments were performed in order to confirm that zinc ion has a stabilizing effect on the structure of hHep1 (Fig. 5B). In the absence of EDTA, a main transition centered at 74 °C was observed, which was attributed to the unfolding of the zinc-finger core, since it was affected by the presence of 2 mM EDTA. The presence of the divalent ion chelating agent led hHep1 to unfold thermally with a transition centered at 69 °C, about 5 °C less than in the absence of EDTA. These results confirm that zinc ion acts by stabilizing the hHep1 structure. In both cases, the thermal-induced unfolding was irreversible, and the curve fitting to extract the apparent enthalpy change of the transition was not performed. Moreover, a transition centered at 50 °C was also observed in both thermograms. This unfolding transition was attributed to the first unfolding event, as also seen in the urea-induced unfolding followed by fluorescence, which was not disturbed by the presence of 2 mM EDTA.

Moreover, urea-induced experiments of hHep1 at 3.5 mg mL^{-1} in the absence and presence of 2 mM EDTA were also monitored by means of SAXS. As hHep1 solutions are a mixture of several oligomeric species, SAXS signal and parameters like MM and R_g depend on the sum of the contribution of each species in solution. As it is not possible to define the scattering contribution

of each species in solution, we cannot apply shape reconstruction modeling based on the particle scattering pattern. However, when we monitored a weighted-average R_g (determined from the Guinier's Law [33]) as a function of urea concentration, a dual behavior was observed: (a) an initial and consistent decrease of the weighted-average R_g up to 4 M urea and, (b) an increment of the weighted-average R_g between 4–6 M Urea (Fig. 5C). In presence of 2 mM EDTA, hHep1 urea-induced unfolding also showed a similar effect, but the initial reduction of the weighted-average R_g-value was observed up to 2 M urea, followed by the increment at higher urea concentrations. Thus, the presence of EDTA led hHep1 to unfold at smaller urea concentrations in agreement with the urea-induced unfolding experiments (Fig. 5A).

The aforementioned dual effect can be explained by the presence of oligomers in the hHep1 solution. The initial decrease of the weighted-average R_g-values involves the dissociation of hHep1 oligomers, concomitant with the unfolding of hHep1 to the intermediate at 2 M urea. This interpretation is consistent with the gradual transition observed in the urea-induced experiments followed by fluorescence (Fig. 5A), and with the dependence on $\langle\lambda\rangle$-signal with protein concentration (Fig. 4). At higher urea concentration (i.e.,>4 M), the hHep1 zinc-finger core unfolds, resulting in an increment of the weighted-average R_g-values, as shown earlier [34], since it was susceptible to the presence of EDTA.

On the whole, the results presented here indicate that the zinc ion acts by stabilizing the hHep1 structure and is in line with the functional results. It was shown that modifications in the zinc finger motifs of yHep1 resulted in defective growth in yeast [17], and the dependence on the zinc finger domain for the proper hHep1 function [21].

4. Concluding remarks

The mitochondrial molecular chaperones, coordinated by mtHsp70, play a key role in the mitochondrial protein import system, since it is the motor that drives the preprotein import process and assists the folding of imported proteins. However, several mtHsp70 are prone to self-aggregation *in vivo* and *in vitro*, which limits their study. Similar to other Hsp70s, mtHsp70s are assisted by many co-chaperones [6,35], with Hep1 being described as an essential mitochondrial co-chaperone. One of the functions of Hep1 is blocking the self-aggregation process of mtHsp70, enabling their maintenance in solution. As shown for other mtHsp70 (and here), recombinant human mortalin depends on hHep1 for soluble expression in *E. coli* cells [18,19,21]. The human mortalin and hHep1 coexpression strategy allows mortalin production and purification as a monomer (data not shown), which will allow future structure-function characterization of mortalin.

Little is known about the structure-function of hHep1. Thus, the goal of this study was to produce the recombinant hHep1 for structure-function characterization. Recombinant hHep1 was purified until homogeneity in the folded state, exhibiting β-sheets as it main secondary structure content, which is in agreement with the molecular homology model built (Fig. 1D).

As observed by AUC and SAXS experiments, hHep1 oligomerizes in dependence on the protein concentration. Hydrodynamic characterization strongly suggested that hHep1 is a mixture of at least three oligomeric species in equilibrium with the monomer. Furthermore, the monomer is the main species in solution, at least at the range of hHep1 concentration studied. However, it remains an open question if hHep1 oligomeric species are essential for its biological function as a co-chaperone of mortalin or mitochondria genesis. The relationship of intrinsic fluorescence emission signal with protein concentration indicates that the oligomerization surface can involve the Trp115 surface region of the hHep1 structure. In fact, Trp115 seems to be protected from the solvent during oligomerization process (Fig. 4). The hHep1 molecular homology model (Fig. 1D) indicates that Trp115 is partially buried between the two α-helices on the C-terminal, thus we can speculate that these structural elements could be involved in the hHep1 oligomerization process.

Human Hep1 is a zinc-finger protein, as observed for ortholog proteins [16,17,21,22]. In order to analyze the structural importance of the zinc ion for hHep1, we performed chemical- and thermal-induced unfolding experiments in the absence and presence of 2 mM EDTA. In all experiments, hHep1 was less stable in the presence of EDTA, suggesting that zinc ion plays a structural role in stabilizing the hHep1.

In sum, the results presented here suggest that, despite the apparent simplicity due to size and function, hHep1 presents a surprising structural behavior and complexity. We also observed that hHep1 shares some structural similarities (secondary structure and monomer's hydrodynamic shape) with the yeast ortholog despite their low identity and functional differences. Further studies must consider the role of the hHep1 oligomerization for its functionality in mortalin regulation and aggregation avoidance.

Acknowledgments

J.C. Borges thanks FAPESP (Fundação de Amparo à pesquisa do Estado de São Paulo) for financial support (grant #2007/05001-4) and CNPq (Conselho Nacional de Pesquisa e Desenvolvimento) for the Research Fellowship grant. L.R.S. Barbosa also thanks to CNPq and FAPESP for financial support. We acknowledge the Spectroscopy and Calorimetry Laboratory at Brazilian Biosciences National Laboratory (LNBio/CNPEM-ABTLuS, Campinas, Brazil) for making available the CD and AUC devices. We also thank the Brazilian Synchrotron Light Laboratory (LNLS/CNPEM-ABTLuS, Campinas, Brazil) for the use of the SAXS beamline.

Appendix A. Supplementary data

Supplementary data associated with this article can be found, in the online version, at http://dx.doi.org/10.1016/j.ijbiomac.2013.02.009.

References

[1] A.C.Y. Fan, J.C. Young, Protein and Peptide Letters 18 (2011) 122–131.
[2] P. Dolezal, V. Likic, J. Tachezy, T. Lithgow, Science 313 (2006) 314–318.
[3] D. Mokranjac, W. Neupert, BBA – Molecular Cell Research 1793 (2009) 33–41.
[4] M. Bohnert, N. Pfanner, M. van der Laan, FEBS Letters 581 (2007) 2802–2810.
[5] P. Rehling, K. Brandner, N. Pfanner, Nature Reviews Molecular Cell Biology 5 (2004) 519–530.
[6] K.P. da Silva, J.C. Borges, Protein and Peptide Letters 18 (2011) 132–142.
[7] S.C. Kaul, C.C. Deocaris, R. Wadhwa, Experimental Gerontology 42 (2007) 263–274.
[8] C. Soti, E. Nagy, Z. Giricz, L. Vigh, P. Csermely, P. Ferdinandy, British Journal of Pharmacology 146 (2005) 769–780.
[9] C.C. Deocaris, N. Widodo, B.G. Shrestha, K. Kaur, M. Ohtaka, K. Yamasaki, S.C. Kaul, R. Wadhwa, Cancer Letters 252 (2007) 259–269.
[10] R. Wadhwa, S. Takano, K. Kaur, C.C. Deocaris, O.M. Pereira-Smith, R.R. Reddel, S.C. Kaul, International Journal of Cancer 118 (2006) 2973–2980.
[11] R. Wadhwa, T. Sugihara, A. Yoshida, H. Nomura, R.R. Reddel, R. Simpson, H. Maruta, S.C. Kaul, Cancer Research 60 (2000) 6818–6821.
[12] R. Wadhwa, T. Yaguchi, K. Hasan, Y. Mitsui, R.R. Reddel, S.C. Kaul, Experimental Cell Research 274 (2002) 246–253.
[13] L.K.S. Szklarz, B. Guiard, M. Rissler, N. Wiedemann, V. Kozjak, M. van der Laan, C. Lohaus, K. Marcus, H.E. Meyer, A. Chacinska, N. Pfanner, C. Meisinger, Journal of Molecular Biology 351 (2005) 206–218.
[14] M. Sichting, D. Mokranjac, A. Azem, W. Neupert, K. Hell, EMBO Journal 24 (2005) 1046–1056.
[15] A.V. Goswami, B. Chittoor, P. D'Silva, Journal of Biological Chemistry 285 (2010) 19472–19482.
[16] L. Burri, K. Vascotto, S. Fredersdorf, R. Tiedt, M.N. Hall, T. Lithgow, Journal of Biological Chemistry 279 (2004) 50243–50249.
[17] H. Yamamoto, T. Momose, Y. Yatsukawa, C. Ohshima, D. Ishikawa, T. Sato, Y. Tamura, Y. Ohwa, T. Endo, FEBS Letters 579 (2005) 507–511.

[18] P. Zhai, C. Stanworth, S. Liu, J.J. Silberg, Journal of Biological Chemistry 283 (2008) 26098–26106.
[19] P. Zhai, M.T. Vu, K.G. Hoff, J.J. Silberg, Biochemical and Biophysical Research Communications 408 (2011) 589–594.
[20] M. Blamowska, M. Sichting, K. Mapa, D. Mokranjac, W. Neupert, K. Hell, Journal of Biological Chemistry 285 (2010) 4423–4431.
[21] M.T. Vu, P. Zhai, J. Lee, C. Guerra, S. Liu, M.C. Gustin, J.J. Silberg, Protein Science 21 (2012) 258–267.
[22] T. Momose, C. Ohshima, M. Maeda, T. Endo, EMBO Reports 8 (2007) 664–670.
[23] M.G. Claros, P. Vincens, European Journal of Biochemistry 241 (1996) 779–786.
[24] K. Arnold, L. Bordoli, J. Kopp, T. Schwede, Bioinformatics 22 (2006) 195–201.
[25] G. Bohm, R. Muhr, R. Jaenicke, Protein Engineering 5 (1992) 191–195.
[26] P. Schuck, M.A. Perugini, N.R. Gonzales, G.J. Howlett, D. Schubert, Biophysical Journal 82 (2002) 1096–1111.
[27] J.C. Borges, C.H.I. Ramos, Current Medicinal Chemistry 18 (2011) 1276–1285.
[28] D. Orthaber, A. Bergmann, O. Glatter, Journal of Applied Crystallography 33 (2000) 218–225.
[29] C.M. Torres-Bugeau, C.L. Ávila, R. Raisman-Vozari, D. Papy-Garcia, R. Itri, L.R.S. Barbosa, L.M. Cortez, V.L. Sim, R.N. Chehín, Journal of Biological Chemistry 287 (2012) 2398–2409.
[30] E. Mylonas, D.I. Svergun, Journal of Applied Crystallography 40 (2007) S245–S249.
[31] O. Glatter, O. Kratky, Small Angle X-Ray Scattering, Academic Press Inc. Ltd., New York, 1982, pp. 17–50.
[32] L.R.S. Barbosa, M.G. Ortore, F. Spinozzi, P. Mariani, S. Bernstorff, R. Itri, Biophysical Journal 98 (2010) 147–157.
[33] G. Fournet, A. Guinier, Small Angle Scattering of X-rays (C.B. Walker, K.L. Yudowitch, Trans.), John Wiley & Sons, New York, 1955, pp. 7–78.
[34] P.R. Dores-Silva, E.R. Silva, F.E.R. Gomes, K.P. Silva, L.R.S. Barbosa, J.C. Borges, Archives of Biochemistry and Biophysics 520 (2012) 88–98.
[35] C.L.P. Oliveira, J.C. Borges, I.L. Torriani, C.H.I. Ramos, Archives of Biochemistry and Biophysics 449 (2006) 77–86.